Received: 24 February 2021 | Revised: 2 October 2021 | Accepted: 6 October 2021

DOI: 10.1111/gbi.12478

ORIGINAL ARTICLE

gebiology WILEY

Contrasting nutrient availability between marine and brackish waters in the late Mesoproterozoic: Evidence from the Paranoá Group, Brazil

Eva E. Stüeken[1] | Sebastian Viehmann[2,3] | Simon V. Hohl[4]

[1]School of Earth & Environmental Sciences, University of St Andrews, St Andrews, UK

[2]Department of Geology, University of Vienna, Vienna, Austria

[3]Department of Lithospheric Research, University of Vienna, Vienna, Austria

[4]State Key Laboratory of Marine Geology, Tongji University, Shanghai, China

Correspondence
Eva E. Stüeken, School of Earth & Environmental Sciences, University of St Andrews, UK.
Email: ees4@st-andrews.ac.uk

Funding information
Natural Environment Research Council, Grant/Award Number: NE/V010824/1 and 41950410566; School of Earth & Environmental Sciences at St Andrews

Abstract

Understanding the delayed rise of eukaryotic life on Earth is one of the most fundamental questions about biological evolution. Numerous studies have presented evidence for oxygen and nutrient limitations in seawater during the Mesoproterozoic era, indicating that open marine settings may not have been able to sustain a eukaryotic biosphere with complex, multicellular organisms. However, many of these data sets represent restricted marine basins, which may bias our view of habitability. Furthermore, it remains untested whether rivers could have supplied significant nutrient fluxes to coastal habitats. To better characterize the sources of the major nutrients nitrogen and phosphorus, we turned to the late Mesoproterozoic Paranoá Group in Brazil (~1.1 Ga), which was deposited on a passive margin of the São Francisco craton. We present carbon, nitrogen and sulphur isotope data from an open shelf setting (Fazenda Funil) and from a brackish-water environment with significant riverine input (São Gabriel). Our results show that waters were well-oxygenated and nitrate was bioavailable in the open ocean setting at Fazenda Funil; the redoxcline appears to have been deeper and further offshore compared to restricted marine basins elsewhere in the Mesoproterozoic. In contrast, the brackish site at São Gabriel received only limited input of marine nitrate and sulphate. Nevertheless, previous reports of acritarchs reveal that this brackish-water setting was habitable to eukaryotic life. Paired with previously published cadmium isotope data, which can be used as a proxy for phosphorus cycling, our results suggest that complex organisms were perhaps not strictly dependent on marine nutrient supplies. Riverine influxes of P and possibly other nutrients likely rendered coastal waters perhaps equally habitable to the Mesoproterozoic open ocean. This conclusion supports the notion that eukaryotic organisms may have thrived in brackish or perhaps even freshwater environments.

KEYWORDS
continental versus marine environments, eukaryotes, Mesoproterozoic, nutrients

1 | INTRODUCTION

The Mesoproterozoic era (ca. 1.6–1.0 Ga), which was bracketed by major biological, chemical and climatic perturbations associated with global oxygenation events in the Paleo- and Neoproterozoic (Lyons et al., 2014), was crucial for the evolution of our biosphere because it saw the appearance and initial radiation of eukaryotic life as indicated by numerous occurrences of eukaryotic microfossils (e.g. Adam et al., 2017; Beghin et al., 2017; Buick & Knoll, 1999; Javaux et al., 2001; Knoll & Nowak, 2017; Pang et al., 2020; Strother et al., 2011). These fossils tend to occur mostly in shallow marine and possibly lacustrine environmental settings, which may be due to persistently anoxic conditions at depth. Deep marine anoxia has been invoked to explain the delayed rise of metazoans (Reinhard et al., 2016), and it probably also hindered the expansion of the first more complex eukaryotic organisms. Several data sets indicate that throughout most of the mid-Proterozoic only land surfaces and the surface ocean were mildly oxygenated (Gutzmer & Beukes, 1998; Hardisty et al., 2017; Sindol et al., 2020), while the deep ocean was largely ferruginous with a low sulphate reservoir (Gilleaudeau & Kah, 2015; Kah et al., 2004; Luo et al., 2014; Planavsky et al., 2011; Poulton et al., 2010). Sulphidic (euxinic) conditions likely existed in upwelling zones along continental margins, and occasional entrainment of sulphide into surface waters may have further restricted the habitat of complex eukaryotic organisms. In a globally anoxic ocean, several essential nutrients may have been limiting, because remineralization of organic matter was suppressed, base metals were trapped in sulphide minerals, phosphorus was efficiently scavenged by ferrous iron, and nitrate was more rapidly reduced to N_2 gas (Derry, 2015; Kipp & Stüeken, 2017; Koehler et al., 2017; Reinhard et al., 2013, 2017; Stüeken, 2013). This emerging view of the mid-Proterozoic ocean can explain the protracted expansion of eukaryotic life into open marine realms; however, it also raises the new question of whether the deep ocean was indeed a significant nutrient source at the time, similar to modern upwelling zones, or if organisms were instead mostly reliant on terrestrial nutrient runoff.

To address this question, we turned to the late Mesoproterozoic Paranoá Group in central Brazil. This unit contains interbedded stromatolitic carbonate and siliciclastic intervals in which previous workers identified diverse assemblages of microfossils, including cyanobacteria and acritarchs (Fairchild et al., 1996). Trace elements and cadmium isotope data from the carbonate units indicate deposition under an oxygenated water column (Viehmann et al., 2019). Importantly, the strata include facies from an open shelf setting that was well connected to the open ocean as well as stromatolites formed in a brackish waters with limited seawater exchange and evidence of significant riverine influence on water chemistry (Section 2). The Paranoá Group thus allows us to compare and contrast living conditions for eukaryotic life under the influences of marine and riverine input. To do so, we analysed samples of stromatolitic carbonate beds for organic carbon, nitrogen and sulphur isotopes. Samples were taken from two field localities: Fazenda Funil and São Gabriel, which are thought to represent an open subtidal and an intertidal lagoon environment, respectively (Viehmann et al., 2019).

2 | GEOLOGICAL SETTING

Chemical and siliciclastic sedimentary rocks of the Mesoproterozoic Paranoá Group were deposited along a passive continental margin of the São Francisco Craton and crop out in mid-eastern Brazil in the state of Goiás. The Paranoá Group unconformably overlies ca. 1.77 Ga Paleoproterozoic (meta)sedimentary rocks of the Araí Group and is unconformably overlain by the Jequitaí diamictitite of the <0.74 Ga old Bambuí Group (Alvarenga et al., 2014; Pimentel et al., 1999, 2011). Age constraints suggest a late Mesoproterozoic to earliest Neoproterozoic depositional age for the Paranoá Group based on Sr-C isotope chemostratigraphy (Alvarenga et al., 2014). The maximum deposition age is further constrained to 1.54 Ga by U-Pb dating of detrital zircons (Matteini et al., 2012). Diagenetic xenotime overgrowth of zircons, dated with Lu-Hf, indicates a minimum depositional age of ~1.04 Ga (Matteini et al., 2012). Biostratigraphy, specifically microfossil assemblages and the occurrence of the *Conophyton metulum* Kirichenkio in the upper Paranoá Group and point to an age bracket of 0.9–1.2 Ga (Dardenne et al., 1976; Fairchild et al., 1996). Taken together, the age is therefore best constrained to a range from 1.0 to 1.2 Ga.

The sedimentary strata of the Paranoá Group are approximately 1000 m thick and divided into nine lithostratigraphic units that were deposited during two transgressive and one regressive cycle (Alvarenga et al., 2014; Campos et al., 2012). Most of the Paranoá Group is made up of siliciclastic rocks including sandstones, siltstone-sandstone rythmites and shales. Dolo- and limestone lenses, which were the focus of this study, occur within the rythmite. These lenses are several tens of metres thick and extend over hundreds of metres along strike (Alvarenga et al., 2014). They are interfingered with pelitic and psammitic rocks, which also occur as intraclasts (Campos et al., 2012). In outcrop, the carbonate units are classed as mudstones and intraclastic grainstones, packstones and floatstones with local conical or columnar and rarely dome-shaped stromatolites. Campos et al. (2012) proposed that the carbonate lenses represent topographic highs during the time of deposition. Tidal indicators within the siliciclastic sedimentary rocks, as well as micritic rip-up clasts from some of the carbonates (Campos et al., 2012) suggest that—with important exceptions highlighted below—sediment deposition largely occurred on an open platform environment with frequent storm events and sporadic subaerial exposure (de Morrison Valeriano, 2016). The stromatolitic strata investigated in this study come from the upper part of the Paranoá Group and were deposited during the second transgression cycle (Campos et al., 2012). Samples were collected at two localities (Figure 1): Fazenda Funil (46°56.4′W, 15°46.9′S) and São Gabriel (47°35.5′W, 15°14.1′S). The conical stromatolites (*Conophyton metulum* Kirichenko) from Fazenda Funil are thought to have been deposited on an open platform, as indicated by tidal features in associated siliciclastic rocks and storm rip-up clasts within the carbonate lens, as described above (Campos et al., 2012; de Morrison Valeriano, 2016).

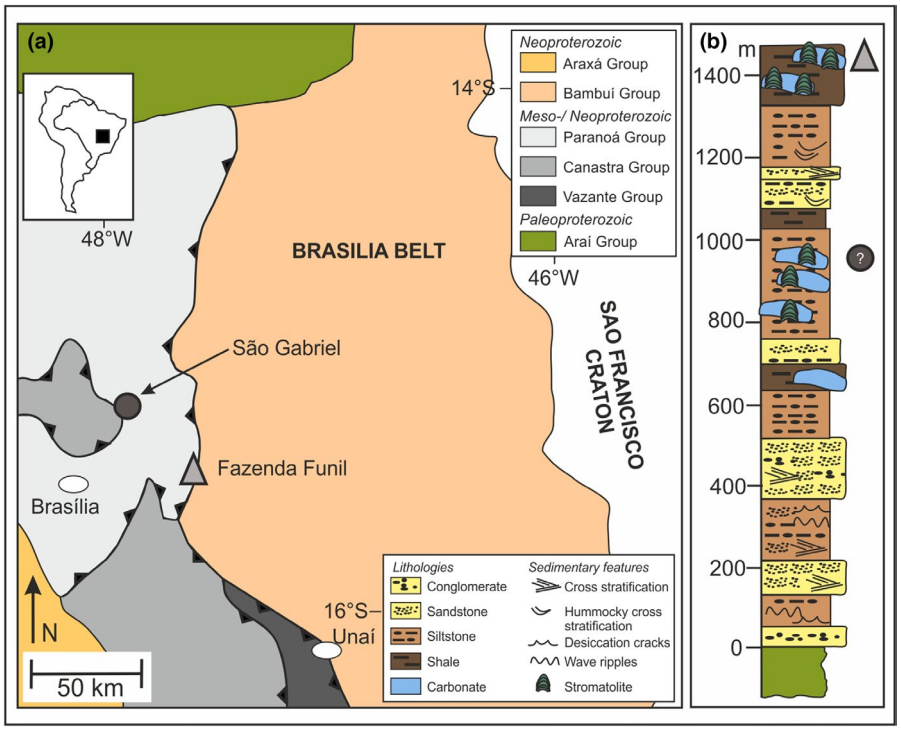

FIGURE 1 (a) Simplified geological map of the field locality in Brazil; (b) Stratigraphic section through the Paranoá Group. The grey triangle and circle indicate our sampling sites. Modified from Viehmann et al. (2019)

The conical morphology of the stromatolites suggests a water depths of around 20 m (Alvarenga et al., 2014; Campos et al., 2012). In contrast, the dome-shaped stromatolites and planar microbialites from São Gabriel are thought to represent shallower water depth (Campos et al., 2012). Carbonates from this setting are flat-laminated, and storm indicators are absent (Fairchild et al., 1996). The depositional setting of São Gabriel has therefore been interpreted as a restricted lagoon. Eukaryotic microfossils have been documented at this locality (Fairchild et al., 1996). The entire sedimentary package has been only weakly metamorphosed (below greenschist facies, Fuck et al., 1988).

The environmental contrast between the two settings is further supported by trace elements and cadmium isotope data from the carbonates (excluding detrital siliciclastic contributions), as shown by Viehmann et al. (2019). These data show a typical marine signature for Fazenda Funil with depletion in shale-normalized (SN) light rare earth elements (REE, Yb_{SN}/Pr_{SN} = 2.1–3.9), strongly superchondritic Y/Ho ratios (37.9–46.2) and fractionated Cd isotopes ($\varepsilon^{112/110}Cd$ = −3.5 to +3.8 units, where $\varepsilon^{112/110}Cd = [(^{112}Cd/^{110}Cd)_{sample}/(^{112}Cd/^{110}Cd)_{standard}-1] \times 10{,}000$, and the 'zero reference' standard is NIST SRM 3108. Note that this ε-notation can be converted to the more familiar δ-notation by dividing by 10, meaning that $\delta^{112}Cd$ in these rocks falls between −0.35‰ and +0.38‰). In contrast, domal stromatolites from São Gabriel show light REE enrichment ($Yb_{SN}/Pr_{SN} < 0.84$) and weakly developed superchondritic Y/Ho ratios (33.6–39.3), Gd_{SN} anomalies ($Gd/Gd^* = 1.1$ to 1.3) and near crustal $\varepsilon^{112/110}Cd$ values (−0.54 to −0.17 ε-units). We note that normalizing the REY inventory of São Gabriel stromatolites to local, ambient hinterland rocks instead of to the commonly used PAAS (Post Archean Australian Shale) results in typical seawater-like REY patterns for these rocks (Viehmann et al., 2019); however, 'seawater-like' REY patterns can already develop in freshwater environments even with minute amount of seawater (5%–10%, Tepe & Bau, 2016). The data are therefore best explained by a scenario where the São Gabriel stromatolites grew in a setting that experienced significant riverine input from the hinterland paired with occasional flooding by seawater (Viehmann et al., 2019). Overall, these geochemical trends are thus strong evidence for two distinct water masses. In other words, the geochemistry supports the sedimentological interpretation that São Gabriel was deposited further inland, perhaps in a lagoon or estuarine setting, compared to Fazenda Funil. This study site is therefore ideal for comparing nutrient sources to the late Mesoproterozoic biosphere. We used carbon and sulphur isotopes to gain further insights into the depositional settings and nitrogen isotopes to reconstruct nitrogen metabolisms. The previously published Cd isotope data can serve as an indirect proxy for phosphorus availability (discussed below). For a detailed petrographic description of these samples, refer to the supplementary files of Viehmann et al. (2019).

3 | METHODS

3.1 | Sampling

Sample descriptions of stromatolites from both the São Gabriel and Fazenda Funil locations studied here directly correspond to those provided by Viehmann et al. (2019). While Viehmann et al. (2019) used

individual stromatolite laminae for trace element and Cd isotope analyses, the sample requirements for this study (several grams) exceeded the amount of individual stromatolite layers. São Gabriel stromatolite laminae are <2 mm in thickness; Fazenda Funil conophyton layers are 0.5 to 3 cm thick. We therefore cut new, larger pieces comprising several laminae out of each stromatolite. Individual stromatolites are listed in Table 1, where secondary indices (lower to higher numbers) correspond to interior, middle and upper parts of individual stromatolites. The subsamples were cut from horizontal stromatolite slabs, using a diamond-bearing saw. Additionally, we analysed pieces of carbonate infill that had formed between stromatolite domes at the São Gabriel location (Table 1). The stromatolite pieces were hammered into mm-sized chips on a steel plate, and the chips were washed in glass beakers with methanol (reagent grade), 1N HCl (reagent grade) and 18 MΩ cm^{-1} DI–H_2O. Each solvent was applied for about 5–10 s and then decanted. The clean chips were dried in a closed oven at 60°C and then pulverized in an agate ball mill.

3.2 | Decarbonation for organic carbon, nitrogen and reduced sulphur analyses

The powder was decarbonated with 2N HCl (reagent grade) in glass centrifuge tubes at 60°C overnight. The next day, the samples were centrifuged and the acid was decanted. A few drops of fresh acid were added to ensure that the samples were no longer reactive, indicating that all carbonate had been dissolved. The residues were then washed with 18 MΩ cm^{-1} DI-H_2O three times and dried at 60°C. The dried residues were stored in scintillation vials. All glassware used during the sample preparation was pre-combusted at 500°C overnight to remove organic matter. With regard to sulphur, this decarbonation protocol removed all carbonate-associated sulphate and any trace sulphate evaporite minerals, leaving behind organic-bound and pyrite-bound sulphide phases. We will therefore refer to it as total reduced sulphur, abbreviated as TRS in the following.

TABLE 1 Organic carbon, nitrogen and sulphur data of decarbonated residues

Identifier	TOC [%]	$\delta^{13}C_{org}$ [‰]	TN [%]	$\delta^{15}N$ [‰]	TS [%]	$\delta^{34}S_{red}$ [‰]	C/N [at.]	C/S [g/g]	$\delta^{34}S_{CAS}$ [‰]	$\delta^{112}Cd$ [‰]
Fazenda Funil (open platform)										
BR-FF-20	1.33	−30.47	0.05	6.68	0.53	8.12	29.56	2.49		
BR-FF-20-1	0.59	−29.79	0.05	6.30	0.52	−0.69	14.26	1.14	24.4	
BR-FF-20-2	0.31	−28.90	0.04	6.40	0.37	1.48	9.52	0.84		0.17 ± 0.05
BR-FF-20-3	1.11	−30.25	0.05	6.77	0.62	5.55	27.21	1.78		*n* = 1
BR-FF-20-4	1.11	−30.47	0.06	6.94	0.45	6.82	23.00	2.46		
BR-FF-30	1.50	−30.90	0.09	6.70	0.44	17.90	19.12	3.43		
BR-FF-30-1	0.58	−30.76	0.06	7.17	0.43	8.97	12.03	1.35		0.01 ± 0.07
BR-FF-30-2	1.73	−29.58	0.11	7.20	0.65	10.05	17.73	2.64		*n* = 3
BR-FF-40	2.42	−30.18	0.13	7.40	0.58	12.99	22.45	4.14		
BR-FF-40-1	2.58	−29.56	0.10	6.85	0.67	13.83	30.23	3.83		
BR-FF-40-2	2.72	−29.61	0.11	6.55	0.65	13.31	30.10	4.16	33.5	−0.23 ± 0.11
BR-FF-40-3	2.22	−30.20	0.10	6.77	0.66	9.60	26.10	3.38		*n* = 5
BR-FF-40-4	1.17	−29.73	0.07	6.85	0.49	7.87	18.64	2.38		
BR-FF-50	0.91	−30.87	0.08	8.38	0.52	8.61	12.60	1.76		
BR-FF-50-1	1.03	−30.29	0.07	7.88	1.23	3.37	17.57	0.84	30.1	0.38 ± 0.05
BR-FF-50-2	0.77	−31.19	0.08	8.25	0.51	8.45	11.89	1.51		*n* = 1
São Gabriel (restricted lagoon)										
BR-SG-1	1.22	−27.04	0.03	2.75	0.25	24.41	41.74	4.86		
BR-SG-Strom-1	2.04	−26.95	0.06	4.42	0.57	25.17	40.10	3.59		−0.06 ± 0.03
BR-SG-carb. infill-1	2.26	−26.81	0.08	4.61	0.35	26.04	32.73	6.51		*n* = 1
BR-SG-2	1.46	−26.90	0.04	3.33	0.44	27.05	42.04	3.34		
BR-SG-Strom-2	1.71	−26.93	0.05	3.45	0.44	26.93	44.17	3.93		−0.02 ± 0.05
BR-SG-carb. infill-2	2.08	−27.05	0.06	3.88	0.49	27.84	39.72	4.23		*n* = 1

Note: Abundances are in weight per cent. at., atomic ratio in units of mol/mol. Average $\delta^{112}Cd$ of same hand specimen carbonate leachate Cd isotopic analyses reported in Viehmann et al. (2019), ±1 SD of multiple (*n*) analyses

3.3 | Carbonate-associated sulphate extraction

For a subset of samples where enough material was available, we extracted carbonate-associated sulphate (CAS). Around 10 g of untreated rock powder was weighed into glass beakers and mixed with roughly 50 ml of concentrated H_2O_2 to oxidize any pyrite contained in the sample (Wotte et al., 2012). The H_2O_2 was left to react for 24 h and then removed with a pipette. Next, the samples were washed with 100 ml of 10% NaCl brine to mobilize sulphate contained in evaporite minerals or produced from pyrite oxidation. The brine was again left for 24 h and then carefully decanted. The residual sample was then washed twice with 18 MΩ cm^{-1} DI-H_2O. To extract CAS, 50 ml of 2N HCl was added to each sample and left to react and occasionally swirled until effervescence had stopped (approximately 30 min). The resulting solution was filtered twice to separate it from residual insoluble solids. The pure solution was then poured back into a clean glass beaker and mixed with 20 ml of 0.5 M $BaCl_2$, which reacts with sulphate to form $BaSO_4$ precipitates. These precipitates were left to settle for 2 days, collected by centrifugation in 50 ml Falcon tubes and washed twice with 18 MΩ cm^{-1} DI-water. The residues were left to dry at 60°C and then analysed as described below.

3.4 | Isotopic analyses

For the C–N–S isotope analysis, the appropriate amount of powder (2–10 mg for decarbonated residues, 0.15–0.20 mg for barite) were weighed into a tin capsule, and 0.5–1.5 mg of V_2O_5 (Elemental Microanalysis) was added as a combustion aid. The capsules were sealed and combusted in an elemental analyser (EA Isolink, Thermo Fisher) that was coupled via a Conflo IV to a gas source isotope-ratio mass spectrometer (MAT253, Thermo Fisher). The EA was equipped with a combustion reactor filled with WO_3 and electrolytic copper, a water trap filled with magnesium perchlorate, and a ramped gas chromatograph oven, which allows measuring all three elements (carbon, nitrogen and sulphur) in one combustion (Sayle et al., 2019; Stüeken et al., 2020). Isotopic data are expressed in delta notation as δ [‰] = [($R_{sample}/R_{reference}$) − 1] × 1000, where $R = {}^{13}C/{}^{12}C$ for carbon, $^{15}N/^{14}N$ for nitrogen and $^{34}S/^{32}S$ for sulphur. The reference standards are VPDB for $\delta^{13}C$, atmospheric N_2 gas for $\delta^{15}N$ and VCDT for $\delta^{34}S$. Isotopic data were calibrated with USGS-40 and USGS-41 for carbon and nitrogen and with IAEA-S2 and IAEA-S3 for sulphur. USGS-42 was used for quality control and gave values of −21.00 ± 0.28‰ for $\delta^{13}C$, +7.99 ± 0.26‰ for $\delta^{15}N$ and +7.55 ± 1.17 ‰ for $\delta^{34}S$, which agree well with the internationally accepted values of −21.09 ± 0.10‰, +8.05 ± 0.10‰ and +7.84 ± 0.25‰ respectively. The large uncertainty in $\delta^{34}S$ in our measurements may be due to heterogeneity in this reference material. For comparison, IAEA-S2 and IAEA-S3 showed a reproducibility in $\delta^{34}S$ of 0.5‰. Peak areas were calibrated for abundances. Average reproducibility for $\delta^{13}C$, $\delta^{15}N$ and $\delta^{34}S$ (1SD) over multiple decarbonated aliquots of the same sample was 0.17‰, 0.50‰ and 1.95‰ respectively. The reproducibility for $\delta^{34}S$ is again relatively poor for our samples, which in this case we attribute to internal heterogeneity within the samples. Because these samples contain over 90% carbonate, separate aliquots had to be decarbonated for replicate analyses, meaning that the variability in our measurements could easily be affected by nugget effects of isotopically heterogeneous pyrite grains. However, the range of measured values far exceeds our uncertainty, meaning that the presented average values are still interpretable.

4 | RESULTS

The analysed samples from the two localities of the Paranoá Group overlap widely in their total organic carbon (TOC, 0.31–2.72 wt.%), total nitrogen (TN, 0.03–0.13 wt.%) and total reduced sulphur (TRS, 0.25–1.23 wt.%) contents in the decarbonated residues (Table 1). However, ratios of organic carbon to total nitrogen (C/N) and organic carbon to sulphur (C/S) are distinct between the two localities. Samples from São Gabriel have on average both higher C/N (40.1 ± 3.9, 1 SD) and higher C/S ratios (4.4 ± 1.2) compared to Fazenda Funil (C/N = 20.1 ± 7.0, C/S = 2.8 ± 1.1, Figure 2). When TN is plotted versus TOC (Figure 2a), both localities show strong correlations ($r^2 = 0.68$ and 0.90), indicating that the nitrogen in these rocks was largely introduced together with organic matter. However, the Fazenda Funil samples have a significant positive TN intercept of 0.037 wt.%, whereas the São Gabriel samples have a small negative TN intercept (−0.018 wt.%, reduces to −0.006 wt.% if one outlier is removed). The rocks from Fazenda Funil therefore contain a slight excess of nitrogen relative to organic carbon.

In terms of organic carbon isotopes ($\delta^{13}C_{org}$), the Fazenda Funil values (−30.1 ± 0.6‰) are on average 3‰ lower than those of São Gabriel (−27.0 ± 0.1‰, Figure 2b). This isotopic offset is mirrored in previously reported carbonate carbon isotope ratios ($\delta^{13}C_{carb}$), which are lower at Fazenda Funil (−1.0 ± 0.2‰) compared to São Gabriel (+2.0 ± 0.1‰) (Viehmann et al., 2019). Nitrogen isotope values ($\delta^{15}N$) are systematically lower at São Gabriel (+3.7 ± 0.7‰) compared to Fazenda Funil (+7.1 ± 0.6‰, Figure 2b), while sulphur isotope values of reduced sulphur ($\delta^{34}S_{red}$) are systematically higher at São Gabriel (+26.2 ± 1.3‰) and lower at Fazenda Funil (+8.5 ± 4.7‰, range −0.7‰ to +17.9‰, Figure 2c). Only three samples from Fazenda Funil yielded sufficient carbonate-associated sulphate for isotopic analyses ($\delta^{34}S_{CAS}$), and the values that we measured were +24.4‰, +30.1‰ and +33.5‰ (Table 1). $\delta^{15}N$ anticorrelates with C/N ratios (Figure 2d), which argues against significant (>1‰) metamorphic alteration of nitrogen isotopes (cf. Haendel et al., 1986; Thomazo & Papineau, 2013), consistent with the sub-greenschist metamorphic grade of these rocks (Fuck et al., 1988).

5 | DISCUSSION

5.1 | Sulphur cycling

Sulphur isotopes are primarily fractionated during microbial sulphate reduction under anoxic conditions, where the resulting sulphide becomes depleted in $\delta^{34}S$ by up to 70 ‰ relative to sulphate (Canfield,

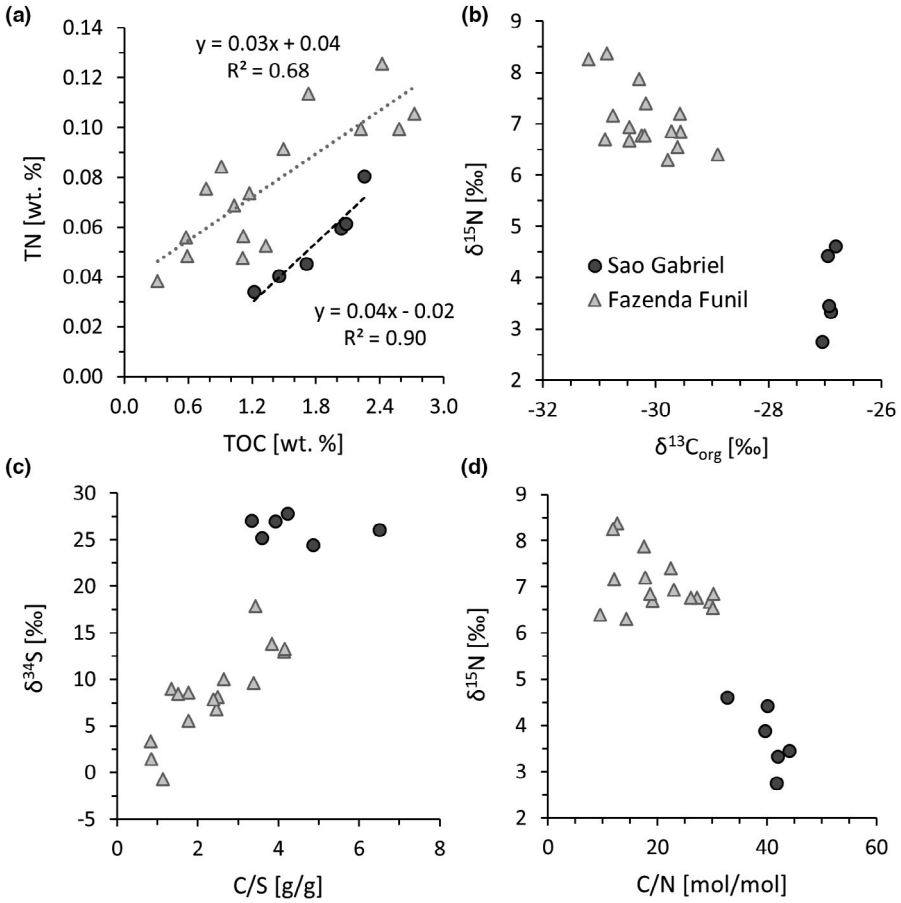

FIGURE 2 Scatter plots of (a) total nitrogen versus total organic carbon; (b) nitrogen isotopes versus organic carbon isotopes; (c) sulphur isotopes versus organic carbon to sulphur ratios; (d) nitrogen isotopes versus organic carbon to nitrogen ratios. Dark grey circles = São Gabriel, light grey triangles = Fazenda Funil

2001; Sim et al., 2011). If sulphate reduction occurs in sedimentary pore waters, it may become diffusion-limited and express strong Rayleigh distillation effects, especially if sulphate concentrations in the overlying water column are less than a few mM (Fike et al., 2015; Gomes & Hurtgen, 2013, 2015). Under these conditions, the residual porewater sulphate becomes progressively enriched in $\delta^{34}S$, as does the produced sulphide (Figure 3a). The isotopic composition of seawater sulphate during the deposition of the Paranoá Group is thus perhaps best estimated by our lowest $\delta^{34}S_{CAS}$ value (+24.4‰). This value falls within the range of previous estimates for late Mesoproterozoic seawater (+20‰ to +30‰, Chu et al., 2007). The two slightly higher $\delta^{34}S_{CAS}$ values of +30.1‰ and +33.5‰ may be part of the isotopic variability that is seen throughout the Proterozoic, when seawater was relatively sulphate-poor (Kah et al., 2004; Luo et al., 2014; Shen et al., 2002); however, it is also possible that these subtle enrichments reflect the effects of Rayleigh fractionation within carbonate-rich sediments, where the residual isotopically enriched sulphate could be trapped as CAS. Similarly, the $\delta^{34}S_{red}$ values between −1‰ and +18‰ in the Fazenda Funil samples are most parsimoniously interpreted as partial sulphate reduction (ca. 45%–55%) under closed-system conditions (Figure 3a). This interpretation is consistent with cadmium isotope data from Viehmann et al. (2019), which revealed diagenetic fractionation effects within an anoxic microbial mat. For the São Gabriel samples, where we were unable to extract CAS from the samples and where the measured $\delta^{34}S_{red}$ values are significantly higher than at Fazenda Funil, sulphate reduction likely progressed further, leading to the complete consumption of the initial sulphate reservoir. This interpretation is consistent with observations from modern anoxic, sulphate-poor lakes, where preserved sulphides approximate the composition of the initial sulphate (Gomes & Hurtgen, 2013, 2015). In Figure 3a, the $\delta^{34}S_{red}$ values from São Gabriel are thus probably best represented by cumulative sulphides at the endpoint of the *x*-axis (0% SO_4^{2-} remaining).

This interpretation would imply that the total sulphate reservoir at the São Gabriel site was smaller (and thus more rapidly consumed) than at Fazenda Funil. As indicated by previously published REY data and sedimentology, this setting experienced significant riverine water input and was only occasionally flooded by seawater (Viehmann et al., 2019) (Figure 4). Mesoproterozoic seawater sulphate levels are estimated to have been ≤2 mM (Fakhraee et al., 2019; Kah et al., 2004; Luo et al., 2014) compared to 28 mM in the modern ocean and roughly 0.16 mM in modern rivers (Burke et al., 2018). These constraints allow for the possibility that Mesoproterozoic

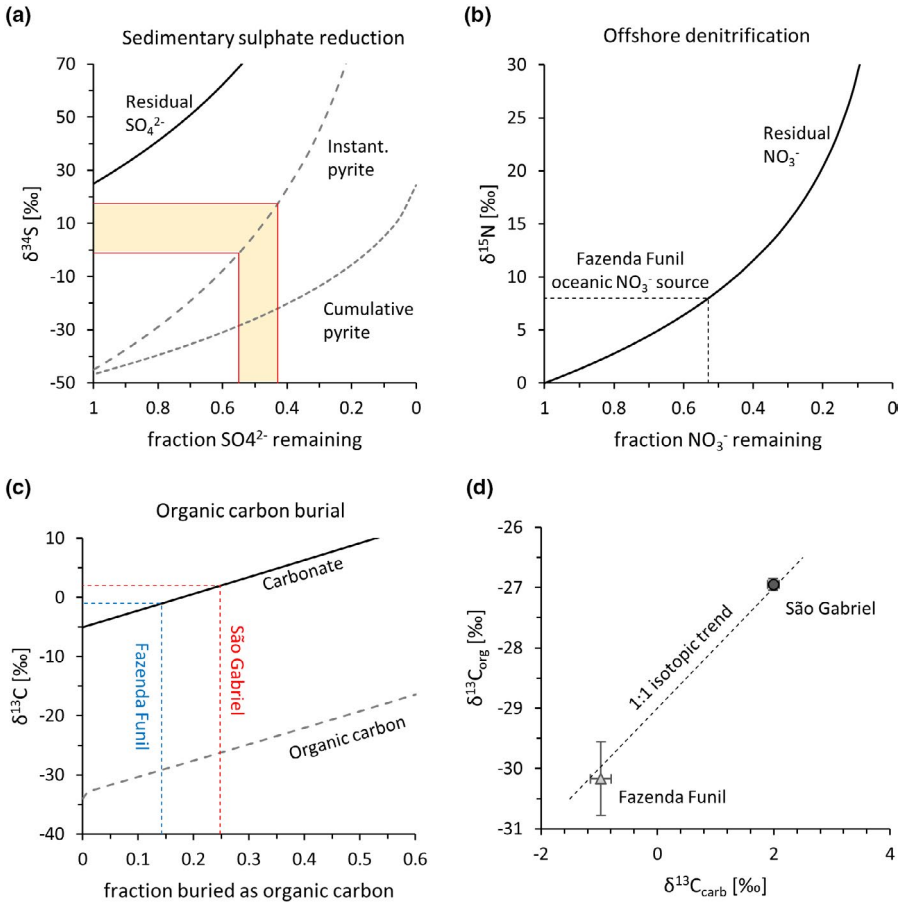

FIGURE 3 Isotopic models. (a) Rayleigh fractionation imparted during microbial sulphate reduction. Orange area corresponds to the reduced sulphur measurements at Fazenda Funil. (b) Rayleigh fractionation imparted during nitrate reduction (denitrification) occurring offshore at the redoxcline. The dashed line shows the degree of denitrification that needed to occur to generate a nitrate pool with a composition of +8‰. (c) Equilibrium carbon isotope fractionation during CO fixation and organic carbon burial. Dashed blue and red lines may explain observed organic and inorganic carbon isotope data at the two study sites. (d) Organic carbon versus carbonate carbon isotopes from the two sites. Each data point is the average of all measurements from the respective locality. This approach was taken, because organic and inorganic carbon isotopes were not measured on the exact same sample aliquots. Carbonate carbon data are from Viehmann et al. (2019). The 1:1 trend line marks the expected offset between localities that differ in the rate of organic carbon burial while the fractionation facture during CO_2 fixation is constant (see panel c)

river water and seawater were not as different as they are today in terms of sulphate content; however, our data are best explained if a significant difference existed already at that time. Further support for this interpretation comes from organic carbon to sulphur ratios, which are known to scale with salinity, because less saline waters tend to contain less dissolved sulphate (Berner & Raiswell, 1984; Wei & Algeo, 2019). The higher C/S ratios at São Gabriel relative to Fazenda Funil (Figure 2c) thus probably point towards a less saline water column. An alternative interpretation could be that Fazenda Funil experienced water-column euxinia and is therefore enriched in S relative to TOC (Leventhal, 1983); however, this is unlikely because (a) the C/S ratios at Fazenda Funil fall within the range of average seawater (2–6, Wei & Algeo, 2019), (b) as noted above the $\delta^{34}S_{CAS}$ and $\delta^{34}S_{red}$ values indicate diagenetic sulphate reduction under closed-system conditions rather than open-system sulphate reduction in the water column, and (c) shale-normalized rare earth element and yttrium (REY) patterns of the Fazenda Funil carbonates would show REY remobilization features typical for anoxic environments (cf. Planavsky et al., 2010) rather than the observed typical open ocean seawater-like patterns (Viehmann et al., 2019). Our data thus point towards a relatively sulfate-depleted setting at São Gabriel, controlled by sulfate-poor freshwater input from rivers and only minor contributions of sulfate-enriched seawater from occasional flooding.

5.2 | Carbon cycling

Carbon isotopes are fractionated during CO_2 fixation of primary producers where biomass becomes depleted in $\delta^{13}C$ relative to the CO_2 source (Figure 3c). The magnitude of the fractionation differs between different metabolic pathways, but typically falls around −27 ± 7‰ for average marine biomass (Schidlowski, 2001). If anaerobic organisms are present, especially during diagenesis, they

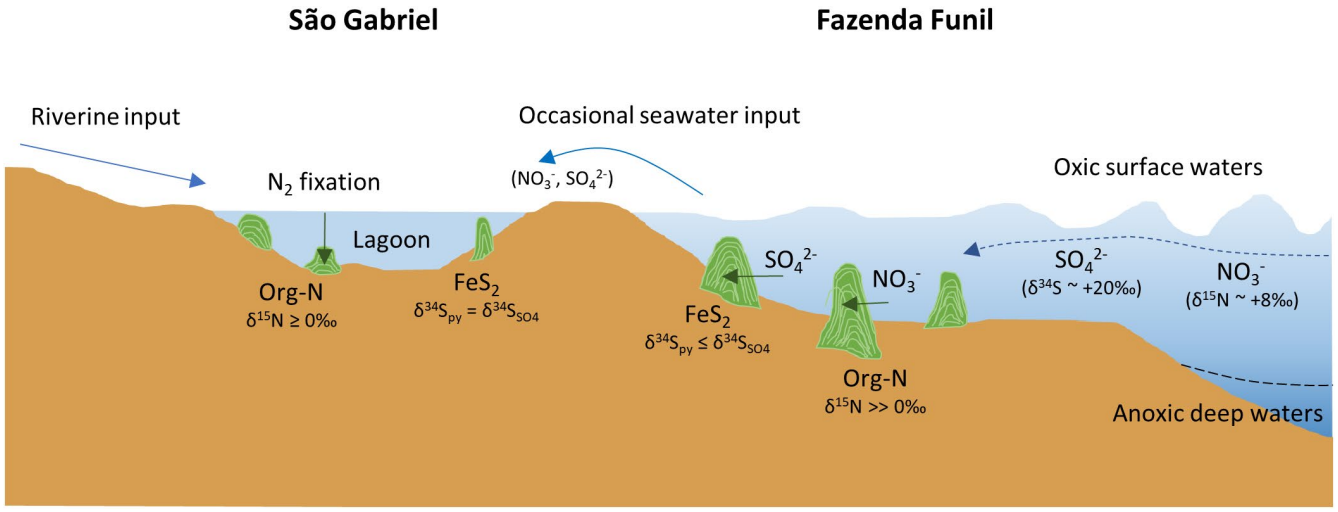

FIGURE 4 Schematic of the inferred sulphur and nitrogen cycle at São Gabriel and Fazenda Funil

may further lower this value by generating and consuming isotopically light methane. This mechanism thus effectively increases the net fractionation between the organic and inorganic carbon phase. Highly negative $\delta^{13}C_{org}$ values in the rock record are therefore typically interpreted as evidence for methane cycling (e.g. Thomazo et al., 2009). In the case of the Paranoá Group, $\delta^{13}C$ values from Fazenda Funil are roughly 3‰ lower than those from São Gabriel, which could indicate that Fazenda Funil hosted a slightly larger proportion of anaerobes within sediments. However, when compared to previously published $\delta^{13}C_{carb}$ values from both sites (Viehmann et al., 2019), the fractionation between inorganic and organic carbon remains constant at ca. −29‰ (Figure 3d), that is $\delta^{13}C_{carb}$ values show a similar 3‰ difference between the two sample sets. Instead of invoking a change in the fractionation factor that resulted from diagenetic alteration of biomass, a more parsimonious explanation appears to be that the relative degree of organic carbon burial was slightly elevated at São Gabriel compared to Fazenda Funil, such that the isotopic composition of the dissolved inorganic carbon (DIC) reservoir was pushed to heavier values (Figure 3c). The biomass of primary producers feeding on this isotopically enriched DIC would thus have become enriched as well. If so, then the São Gabriel lagoon—although poorly connected to the global ocean—hosted a highly productive microbial ecosystem.

5.3 | Nitrogen cycling

5.3.1 | Background on nitrogen isotope fractionation

The main source of nitrogen to the biosphere is biological N_2 fixation to ammonium, which typically imparts a small isotopic fractionation of −2‰ to +1‰ (Zhang et al., 2014). During biomass degradation under oxic conditions, such as in the photic zone of the ocean where most biomass turnover occurs (e.g. Burdige, 2007), the ammonium is rapidly oxidized to nitrate with no net isotopic alteration. The resulting nitrate is thus the major species of fixed nitrogen in oxic seawater. In oxygen minimum zones in the water column, dissolved nitrate can be reduced back to N_2 gas by denitrifying microbes (e.g. Lam & Kuypers, 2011), and this process imparts a strong isotopic fractionation of 12.5‰ on average, rendering the residual nitrate reservoir isotopically enriched (Kritee et al., 2012). If, however, denitrification occurs within sedimentary pore waters under diffusion-limited conditions, the net isotopic effect is much smaller (0‰ to 3‰ Kessler et al., 2014; Rooze & Meile, 2016). The ratio of water-column denitrification to sedimentary denitrification therefore controls the average isotopic composition of the marine nitrate reservoir. In the modern ocean, this value is approximately +5‰ reflecting roughly 30% water-column denitrification (Stüeken et al., 2016; Zhang et al., 2020). The $\delta^{15}N$ value of marine nitrate can be archived in the geological record, because nitrate is assimilated into biomass as a major nutrient, and this biomass can be buried and preserved in sediments. $\delta^{15}N$ values of sediment cores from the modern ocean therefore also fall around a mean of +5‰, reflecting the composition of seawater nitrate (Tesdal et al., 2013). This picture changes, however, in anoxic basins, such as the Black Sea, where the nitrate reservoir in surface waters is very small. Here, the biomass of N_2-fixing organisms and ammonium assimilators makes up a significant proportion of buried organic matter, leading to sedimentary $\delta^{15}N$ values close to 0‰ (Fulton et al., 2012). Mixing of biomass from nitrate assimilators and N_2-fixing organisms leads to intermediate values (Kipp et al., 2018; Thunell et al., 2004).

5.3.2 | Nitrogen sources and sinks in the Paranoá basin

In the case of the Paranoá Group, the distinct $\delta^{15}N$ values between the two sampling sites thus indicate differences in nitrogen

metabolisms during the time of deposition. The relatively high values up to +8‰ at Fazenda Funil are most parsimoniously explained as the relics of nitrate-assimilating organisms. In other words, dissolved nitrate was likely present in the water column and bioavailable. To attain a value of +8‰, this nitrate reservoir must have undergone partial denitrification in the water column elsewhere (Figure 3b), possibly along a redox cline in deeper waters further offshore (Figure 4); however, the preservation of the isotopic signature of nitrate in the rock record indicates that the residual amount of nitrate was high enough to sustain a significant fraction of the local ecosystem (Kipp et al., 2018). This residual nitrate pool would have been washed up onto the continental shelf.

Similar to sulphate, the marine nitrate reservoir with a $\delta^{15}N$ of +8‰ probably also periodically spilled into the lagoon at São Gabriel. However, the comparatively lower $\delta^{15}N$ values at this site (mean 3.7 ± 0.7 ‰) suggest that an additional source of isotopically light nitrogen was present. The most likely source is biological N_2 fixation, which would have contributed biomass with a composition around −2‰ to +1‰. Similar to the modern Cariaco basin (Thunell et al., 2004), mixing of biomass from N_2-fixers and nitrate assimilators probably led to an average composition of +3‰ to +4‰. It is also possible that isotopically light nitrate was washed in by rivers, derived from oxidation of microbial mats on land (Thomazo et al., 2018). In any case, our nitrogen isotope data thus suggest that nitrate was bioavailable in the open shelf setting represented by Fazenda Funil, where it may have been supplied by remineralization of organic matter occurring within a deep oxic photic zone. We find no evidence from these data that a riverine input of nitrate was necessary for sustaining life in open marine settings. In contrast, at São Gabriel, where seawater input was intermittent (Viehmann et al., 2019), the eukaryotic ecosystem that has been described from this locality (Fairchild et al., 1996) may have been sustained by a combination of prokaryotic N_2 fixation and possibly riverine nitrate input.

5.3.3 | Considering diagenesis

Diagenesis can alter sedimentary $\delta^{15}N$ values by a few permil (Altabet et al., 1999; Freudenthal et al., 2001; Lehman et al., 2002; Moebius, 2013; Robinson et al., 2012), but the effect is biologically driven and largest in oxic sediments where organic ammonium is partially oxidized to nitrate. In this case, the residual ammonium becomes isotopically enriched in the heavy isotope. Under anoxic conditions, growth of N_2-fixing anaerobes can lower the net $\delta^{15}N$ value (e.g. Lehman et al., 2002). In other words, diagenetic alteration of sedimentary $\delta^{15}N$ is dependent on the environment and therefore part of the environmental signature that we are trying to extract. If the samples from Fazenda Funil were affected by partial ammonium oxidation to nitrate during diagenesis and therefore isotopically enriched, it would only support our overall conclusion that nitrate was present in the water column at this site. However, the relatively lower C/N ratios and the high TN intercept at Fazenda Funil argue against significant aerobic ammonium oxidation, because this process removes organic carbon and nitrogen simultaneously. In contrast, anaerobic biomass degradation coupled to sulphate reduction oxidizes carbon to CO_2 but cannot oxidize ammonium; ammonium oxidation coupled to sulphate reduction is thermodynamically unfeasible, allowing ammonium to build up in pore waters (Stüeken et al., 2016). Subsequent adsorption of this pore water ammonium to clay minerals would thus explain the enrichment in TN in the Fazenda Funil samples (Figure 2a). At São Gabriel, where C/N ratios are higher and the TN enrichment is lower, sulphate-driven biomass degradation was likely less important, consistent with evidence for a smaller sulphate reservoir (Section 5.1) and higher rates of biomass burial (Section 5.2). Hence prior to diagenesis, $\delta^{15}N$ values at São Gabriel may have been lower than what was measured, while at Fazenda Funil pre-diagenetic values were possibly slightly higher or similar to the final archived value. Diagenetic alteration does therefore not impact our overall conclusions.

5.4 | Comparison to other mid-Proterozoic basins

The isotopic properties of the two sampling sites present a self-consistent environmental scenario for the Paranoá basin (Figure 4): Oxic waters rich in nitrate and sulphate flushed around the stromatolites that were growing offshore at Fazenda Funil; nitrate acted as a major nitrogen source to living organisms at this site; sulphate underwent partial reduction during anaerobic diagenesis within microbial mats. In contrast, the more restricted lagoon at São Gabriel only received occasional seawater input and therefore had a limited reservoir of marine nitrate and sulphate. Sulphate was more rapidly and quantitatively consumed during diagenetic reduction, and the marine nitrate limitation was offset by biological N_2 fixation or possibly by an influx of nitrate from land. With regard to sulphur, similar basinal gradients with higher sulphate availability offshore and lower availability onshore have previously been described from other mid-Proterozoic basins. In the Roper basin in northern Australia (~1.4 Ga), $\delta^{34}S$ values of reduced sulphur are depleted down to −20‰ in deep basinal facies and enriched up to +50‰ on the inner shelf (Figure 5) (Shen et al., 2003). In the Taoudeni basin in NW Africa (~1.1 Ga), values within a euxinic wedge offshore along the coast (within the chemocline) drop down to around −20‰ while values from intermittently euxinic deeper waters range from −5 to +35 and samples from shallow waters on the shelf plot between 0 and +20 (Figure 5b) (Gilleaudeau & Kah, 2015). In both cases, the very light values were interpreted as evidence of sulphate reduction within the water column, while the heavy values likely suggest diagenetic sulphate reduction under closed-system conditions. Water-column sulphate reduction is not observed in the Paranoá Group, but the relative enrichment in ^{34}S at both Fazenda Funil and São Gabriel is comparable to the enrichments seen in non-euxinic facies in the Roper and Taoudeni basins and probably explained by the same mechanism of diffusion-limited diagenetic sulphate reduction within sediments.

However, the nitrogen data from the Paranoá Group differ somewhat from those of other mid-Proterozoic basins (Table 2).

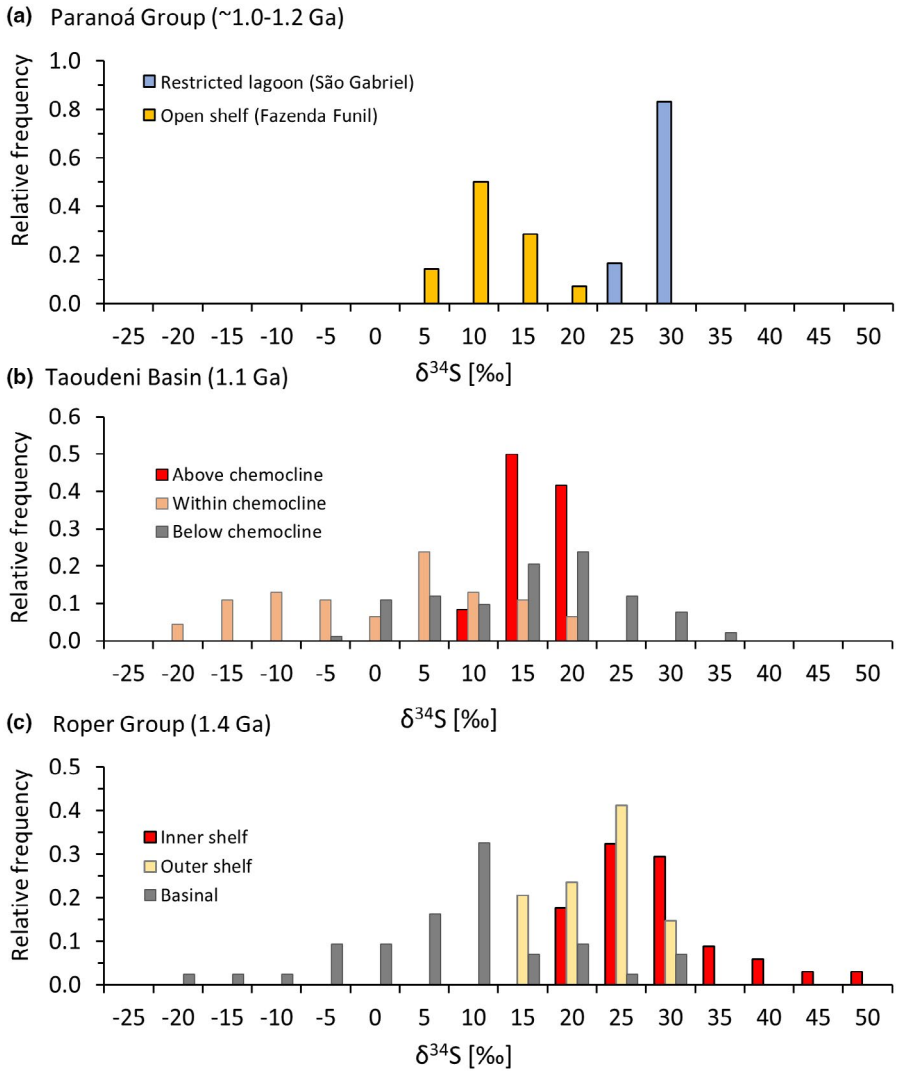

FIGURE 5 Comparison of sulphur isotope data between the Paranoá Group in Brazil (this study), the Taoudeni Basin in NW Africa (Gilleaudeau & Kah, 2015) and the Roper Group in northern Australia (Shen et al., 2003)

TABLE 2 Comparison of $\delta^{15}N$ values between Mesoproterozoic basin.

Unit	Site/sub-unit	Age [Ga]	Setting	$\delta^{15}N$ intertidal	$\delta^{15}N$ subtidal	Ref.
Paranoá Gp	São Gabriel, Fazenda Funil	~1.1	Passive margin	+3.7 ± 0.7	+7.1 ± 0.6	1
Bylot Spgp	Arctic Bay Fm	1.05	Intracontinental graben	+3.5 ± 1.2	+2.4 ± 0.7	2[a]
Vindhyan Spgp	Bijaygarh Shale	1.2	Epicontinental basin		+1.8 ± 0.7	3
Roper Gp	multiple units	1.36–1.5	Epicontinental basin	+3.0 ± 1.7	+2.4 ± 0.9	4
Belt Spgp	Helena Embayment	1.4–1.5	Intracontinental rift	+4.1 ± 1.4	+0.1 ± 0.9	5
Jixian Gp	Gaoyuzhuang Fm	1.56	Epicontinental basin		+7.5 ± 1.5	6
Bangemall Spgp	Edmond Gp	1.5–1.6	Epicontinental basin	+3.5 ± 1.4	+2.1 ± 1.4	4

Note: Each value is the average of multiple analyses for a particular basin and facies, ±1 SD. Blank cells reflect absence of data. Where applicable, data from intermediate facies were excluded. 1. This study, 2. Hodgskiss et al. (2020), 3. Gilleaudeau et al. (2020), 4. Koehler et al. (2017), 5. Stüeken (2013), 6. Wang et al. (2020).

[a]For the intertidal setting of the Arctic Bay Formation, only the lower 600 m of the Alpha River section were considered; the subtidal setting includes the upper Alpha River section and the entire Shale Valley section (Hodgskiss et al., 2020).

$\delta^{15}N$ values in parts of the Belt Supergroup (~1.45 Ga), the Roper Group (~1.4 Ga), the Bangemall Supergroup (~1.55 Ga) and the Bylot Supergroup (1.2 Ga) typically fall around +3‰ to +4‰ in intertidal facies and between 0‰ and +2.5‰ in subtidal facies (Hodgskiss et al., 2020; Koehler et al., 2017; Stüeken, 2013). Subtidal sedimentary rocks from the Vindhyan Supergroup (+1.8‰, 1.05 Ga) also fit into this pattern (Gilleaudeau et al., 2020). Sedimentary lithology is unlikely to play a role, because nitrogen is primarily introduced into sediments via burial of organic matter, independently from the carbonate content. As noted above, some ammonium partitions into clay minerals during diagenesis, but the isotopic fractionation associated with that is small. Hence, the ratio of clays to carbonates is not expected to impart a systematic change on the preserved isotopic value. Therefore, this basinal gradient of nitrogen isotope ratios has been interpreted as evidence that nitrate bioavailability was restricted to shallow waters during the mid-Proterozoic, imposing an additional throttle on the radiation of eukaryotic life (Koehler et al., 2017; Stüeken, 2013). The relatively high values of +7‰ on average from the subtidal setting at Fazenda Funil in the Paranoá Group represent an outlier and are more akin to observations from the Jixian Group (1.56 Ga) (Wang et al., 2020). In the latter case, these values were interpreted as evidence for low biological productivity, which allowed nitrate to accumulate in surface waters further offshore than in other basins. It is possible that a similar explanation applies in the case of the Paranoá Group. Alternatively, the redoxcline that separated oxic surface waters from anoxic deep waters may have been deeper in the Paranoá basin, similar to what has been invoked for the Paleoproterozoic where $\delta^{15}N$ values around +7‰ are frequently observed in offshore facies (Kipp et al., 2018). Importantly, the Paranoá Group was deposited along a passive continental margin rather than in a restricted intracontinental basin. It is therefore conceivable that the Paranoá basin was less stagnant with a deeper mixed layer that pushed the redoxcline to greater depth. Our data may therefore suggest that nitrate was bioavailable in the open shelf settings such as Fazenda Funil without the need for significant fluvial nitrate input. On the other hand, continental settings as represented by São Gabriel were also able to support eukaryotic ecosystems, despite limited access to the marine nitrate pool, indicating that the marine nitrate reservoir was not a necessary requirement for eukaryotic life. In other words, our data suggest that both offshore marine and continental settings contained bioavailable forms of fixed nitrogen, just derived from potentially different sources. From the perspective of nitrogen, continental settings such as São Gabriel may thus have been as habitable as open marine shelf environments.

5.5 | Using Cd isotopes as an indirect proxy for P cycling in the Paranoá basin

The second major nutrient to consider is phosphorus. Phosphorus abundance data from bulk sedimentary rocks are difficult to interpret with regard to bioavailability, due to potential detrital input and diagenetic migration. However, we can make indirect inferences about phosphorus bioavailability between the two sites by looking at the previously published cadmium isotope records. Viehmann et al. (2019) showed that the authigenic (detrital-input corrected) Cd isotopic compositions of carbonate leachates from the Fazenda Funil and São Gabriel stromatolites express considerable fractionation (~7.3 ε units = 0.73 in $\delta^{112}Cd$ space) that exceeds the range of the weathering flux from continental crust into the modern ocean (Schmitt et al., 2009). Cadmium concentrations and its isotopes are gaining increasing traction in biogeochemistry, because they can indirectly record the availability of the macronutrient phosphorus (Abouchami et al., 2014; Boyle et al., 1976; Gault-Ringold et al., 2012; Xie et al., 2019). It has been shown that in highly productive surface waters of the modern ocean, the uptake of Cd by phototrophic organisms leads to an overall depletion of seawater in dissolved Cd concentrations and a shift in isotopic composition of residual Cd to higher values ($\delta^{112}Cd$ of +0.3‰ to +0.5‰) due to the preferential (biological) uptake of the light isotope species into biomass (Conway & John, 2015; Guinoiseau et al., 2019; Lacan et al., 2006; Xie et al., 2019). Under nutrient limited conditions, the remaining dissolved Cd pool becomes isotopically enriched due to Rayleigh fractionation, and this residual enriched Cd reservoir can be preserved in shallow-water carbonates (Hohl et al., 2017). A regeneration of organic-bound Cd in modern deep waters is achieved via oxidation of sinking dead biomass, releasing Cd back into seawater. This remineralization process results in rather homogenous Cd isotopic compositions of $\delta^{112}Cd$ of 0‰ to +0.15‰ in the modern deep oceans (Ripperger et al., 2007; Schmitt et al., 2009; Xie et al., 2019). Importantly, the pathway of biological uptake in the photic zone and remineralization at depth mimics the behaviour of P in seawater, which makes Cd isotopes a promising tool for tracking P cycling in deep time.

In the case of the Paranoá Group, authigenic $\delta^{112}Cd$ values in carbontes from the more continental setting at São Gabriel (-0.02 ± 0.05 ‰ and -0.06 ± 0.03‰) fall close to average continental crust (~0‰, Schmitt et al., 2009) while authigenic $\delta^{112}Cd$ values from the open shelf at Fazenda Funil are significantly fractionated (−0.35‰ to +0.38‰) (Viehmann et al., 2019). The isotopic enrichment at Fazenda Funil is thought to result from Cd uptake into biomass and into sulphide precipitates within microbial mats. According to this model, the highest $\delta^{112}Cd$ values would coincide with maximum Cd depletion of the dissolved Cd pool in pore waters of the ancient microbial mats following Rayleigh-type fractionation patterns (Viehmann et al., 2019). If biological uptake is the major Cd sink, as in the modern ocean, this would mean that Cd isotopes do indeed approximate the behaviour of P and therefore reflect active metabolic depletion of the P reservoir at Fazenda Funil. Alternatively, it is possible that the Cd isotope fractionation observed in these samples was caused predominantly by diagenetic sulphide formation and is therefore not reflective of P availability. For example, Guinoiseau et al. (2018) showed in an experimental set-up that Cd isotope fractionation can be initiated under euxinic marine environments, and Hohl et al. (2019, 2020) found that sulphide precipitation in restricted marine basins alters the overall Cd isotopic composition in the basin waters. To test whether the observed $\delta^{112}Cd$ fractionation

in stromatolitic carbonates is truly biological in origin or initiated by the sulphidic conditions expected within a Proterozoic microbial mat, we averaged the Cd isotope compositions of individual stromatolite laminae of the Fazenda Funil locality reported in Viehmann et al. (2019) and set them into relation to the C, N and S isotopic compositions of the same stromatolite samples analysed in this study (Table 1). This approach was taken, because different amounts of sample material were used for the study of Viehmann et al. (2019) and this study; however, samples of both studies originate from the exact same hand specimens and region of the various stromatolites. The results show that the highest average authigenic δ^{112}Cd values at Fazenda Funil coincide with the highest δ^{15}N ($r^2 = 0.40$) and with the lowest δ^{34}S values ($r^2 = 0.51$) in individual hand specimens (Figure 6), which both indicate relatively oxic conditions with significant available nitrate and sulphate pools. This pattern is opposite to what would be expected from sulphide-induced Cd isotope fractionation. Therefore, the negative correlation between δ^{112}Cd and δ^{34}S may reflect a mixing trend between an isotopically heavy fluid, where the Cd pool is influenced mainly by biological activities under oxic conditions, and an isotopically light fluid with Cd affected by remineralization of organic matter and possibly by limited sulphide precipitation. Biomass remineralization is like the major source of isotopically light Cd, because the fractionation factor during biological uptake is high compared to that of sulphide formation (Hohl et al., 2020). This means that the elevated authigenic δ^{112}Cd values at Fazenda Funil most likely reflect biological consumption of Cd and—by extension from the modern ocean—of dissolved P. Importantly, the modelled Cd isotopic compositions of Proterozoic seawater in this basin (~0.55 δ^{112}Cd units) (Viehmann et al., 2019) overlap with values reported from surface seawaters (SSW) in the modern oceans ($\delta^{112}Cd_{SSW}$ generally between +0.3‰ to +0.5‰) (e.g. George et al., 2019; Sieber et al., 2019; Xie et al., 2019), which further supports our interpretation of similar nutrient cycling and P-uptake in the phototrophic zone.

In contrast, at the São Gabriel locality, authigenic δ^{112}Cd values plot close to crustal values, reflecting a strong influence by riverine nutrient influx that was not significantly affected by subsequent isotopic fractionation. However, we know from the carbon isotope data (Section 5.2) that this setting experienced significant biological activity. Hence, the lack of isotopic fractionation in Cd is unlikely to reflect limited primary productivity. Instead, it is more likely that the dissolved Cd reservoir was too large (and too frequently refreshed) to experience significant isotopic alteration by partial biological uptake of Cd. If correct, this interpretation would imply that other major nutrients, particularly P, whose behaviour appears to mirror that of dissolved Cd in the modern ocean (see above), were relatively abundant in the São Gabriel lagoon. Considering the significant freshwater input to São Gabriel, as indicated by REY data (Viehmann et al., 2019) and sulphur geochemistry (this study), our results therefore suggest that freshwaters were relatively enriched in P, potentially more so than the Mesoproterozoic open ocean, which is thought to have been P-depleted (Reinhard et al., 2017). We stress that the Cd isotope proxy is still in its infancy and more data

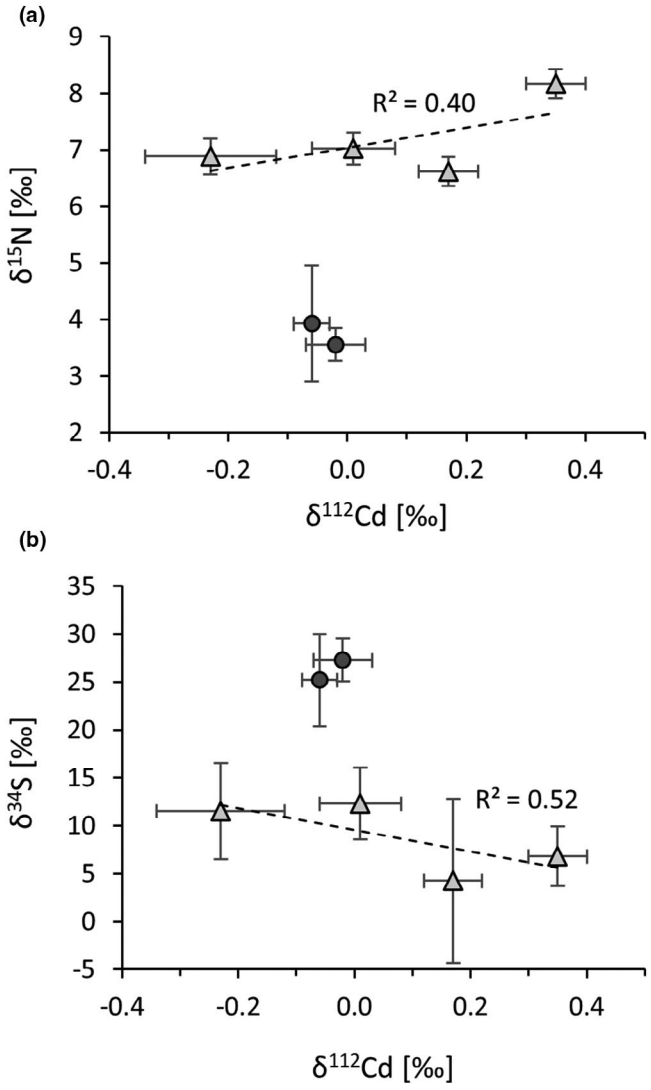

FIGURE 6 Average Cd isotopic compositions obtained on carbonate leachates compared to average nitrogen (a) and sulphur isotopic compositions (b) obtained on same stromatolite hand specimen (error bars represent 1SD within subsamples). Light grey triangles represent Fazenda Funil, and dark grey circles represent Saõ Gabriel

are needed to corroborate its applicability to Proterozoic settings. However, our conclusion is consistent with modelling studies suggesting that Precambrian river waters were P-enriched compared to today and compared to Precambrian seawater (Hao et al., 2017, 2020). Brackish and freshwater settings may therefore have offered important niches for early life.

6 | CONCLUSIONS

The Paranoá Group presents itself as an open marine shelf that was probably well-oxygenated. Sulphate reduction appears to have been limited to sedimentary pore waters, and nitrate was sufficiently bioavailable to sustain a large proportion of the ecosystem. This

environment was thus hospitable to eukaryotic life, as supported by the presence of eukaryotic microfossils. However, the Paranoá Group provides two important nuances to our view of eukaryotic habitats: First, the passive margin environment captured by these rocks may have been better mixed and perhaps more deeply oxygenated than restricted basins; and second, brackish waters such as those represented by São Gabriel were probably equally habitable to complex organisms, as evidenced by eukaryotic acritarchs at this site (Fairchild et al., 1996). Phylogenetic data suggest that some of the first eukaryotes thrived in non-marine environments during the mid-Proterozoic (Sánchez-Baracaldo et al., 2017), but this hypothesis has been difficult to test with geological samples because of the low preservation potential of non-marine sedimentary rocks (Peters & Husson, 2017). The Paranoá cannot fill this gap, but it demonstrates that settings with only intermittent seawater input were inhabited and perhaps not even directly dependent on marine nutrient supplies. In fact, riverine nutrient fluxes may have led to elevated abundances of phosphorus in fresh- and brackish-water settings. To better understand the evolution of eukaryotic life, it may therefore be important to place stronger emphasis on reconstructing riverine nutrient fluxes on the Proterozoic Earth.

ACKNOWLEDGMENTS

EES acknowledges financial support from the School of Earth & Environmental Sciences at St Andrews and from a NERC Frontiers grant (NE/V010824/1). SVH acknowledges funding from the NSFCs Young International Scientist grant, funding no. 41950410566. We thank D.H.G. Walde for organizing the field trip to Fazenda Funil and São Gabriel within the framework of the workshop on molecular fossils and acritarchs from the Neoproterozoic and Lower Paleozoic in Brasilia in 2013.

DATA AVAILABILITY STATEMENT

All data used in this manuscript are presented in Tables 1 and 2 in the manuscript.

ORCID

Eva E. Stüeken https://orcid.org/0000-0001-6861-2490
Sebastian Viehmann https://orcid.org/0000-0001-6138-5862
Simon V. Hohl https://orcid.org/0000-0002-0522-4973

REFERENCES

Abouchami, W., Galer, S. J. G., Baar, H. J. W., de Middag, R., Vance, D., Zhao, Y., Klunder, M., Mezger, K., Feldmann, H., & Andreae, M. O. (2014). Biogeochemical cycling of cadmium isotopes in the Southern Ocean along the Zero Meridian. *Geochimica Et Cosmochimica Acta*, *127*, 348–367. https://doi.org/10.1016/j.gca.2013.10.022

Adam, Z. R., Skidmore, M. L., Mogk, D. W., & Butterfield, N. J. (2017). A Laurentian record of the earliest fossil eukaryotes. *Geology*, *45*, 387–390. https://doi.org/10.1130/G38749.1

Altabet, M. A., Pilskaln, C., Thunell, R., Pride, C., Sigman, D., Chavez, F., & Francois, R. (1999). The nitrogen isotope biogeochemistry of sinking particles from the margin of the Eastern North Pacific. *Deep Sea Research Part I: Oceanographic Research Papers*, *46*, 655–679. https://doi.org/10.1016/S0967-0637(98)00084-3

Alvarenga, C. J., Santos, R. V., Vieira, L. C., Lima, B. A., & Mancini, L. H. (2014). Meso-Neoproterozoic isotope stratigraphy on carbonates platforms in the Brasilia Belt of Brazil. *Precambrian Research*, *251*, 164–180. https://doi.org/10.1016/j.precamres.2014.06.011

Beghin, J., Storme, J. Y., Blanpied, C., Gueneli, N., Brocks, J. J., Poulton, S. W., & Javaux, E. J. (2017). Microfossils from the late mesoproterozoic–early neoproterozoic atar/el Mreïti group, Taoudeni basin, Mauritania, northwestern Africa. *Precambrian Research*, *291*, 63–82. https://doi.org/10.1016/j.precamres.2017.01.009

Berner, R. A., & Raiswell, R. (1984). C/S method for distinguishing freshwater from marine sedimentary rocks. *Geology*, *12*, 365–368.

Boyle, E. A., Sclater, F., & Edmond, J. M. (1976). On the marine geochemistry of cadmium. *Nature*, *263*, 42–44. https://doi.org/10.1038/263042a0

Buick, R., & Knoll, A. H. (1999). Acritarchs and microfossils from the Mesoproterozoic Bangemall Group, northwestern Australia. *Journal of Paleontology*, *73*, 744–764. https://doi.org/10.1017/S0022336000040634

Burdige, D. J. (2007). Preservation of organic matter in marine sediments: Controls, mechanisms, and an imbalance in sediment organic carbon budgets? *Chemical Reviews*, *107*, 467–485.

Burke, A., Present, T. M., Paris, G., Rae, E. C. M., Sandilands, B. H., Gaillardet, J., Peucker-Ehrenbrink, B., Fischer, W. W., McClelland, J. W., Spencer, R. G. M., Voss, B. M., & Adkins, J. F. (2018). Sulfur isotopes in rivers: Insights into global weathering budgets, pyrite oxidation, and the modern sulfur cycle. *Earth and Planetary Science Letters*, *496*, 168–177. https://doi.org/10.1016/j.epsl.2018.05.022

Campos, J. E. G., Bogossian, J., & Carvalho, R. M. (2012). Sedimentology of the Psammo-pelitic-carbonate Unit, Paranoá Group, and Sete Lagoas Formation, Bambuí Group: examples of mixed carbonate-siliciclastic sedimentation in the Proterozoic of the Brasília Fold Belt. *Revista Brasileira De Geociências*, *42*, 513–522. https://doi.org/10.25249/0375-7536.2012423513522

Canfield, D. E. (2001). Biogeochemistry of sulfur isotopes. *Reviews in Mineralogy and Geochemistry*, *43*, 607–636. https://doi.org/10.2138/gsrmg.43.1.607

Chu, X., Zhang, T., Zhang, Q., & Lyons, T. W. (2007). Sulfur and carbon isotope records from 1700 to 800 Ma carbonates of the Jixian section, northern China: Implications for secular isotope variations in Proterozoic seawater and relationships to global supercontinental events. *Geochimica Et Cosmochimica Acta*, *71*, 4668–4692. https://doi.org/10.1016/j.gca.2007.07.017

Conway, T. M., & John, S. G. (2015). Biogeochemical cycling of cadmium isotopes along a high-resolution section through the North Atlantic Ocean. *Geochimica Et Cosmochimica Acta*, *148*, 269–283. https://doi.org/10.1016/j.gca.2014.09.032

Dardenne, M. A., Faria, A., & Andrade, G. F. (1976). Occurrence de stromatolithes columnaires dans le Groupe Bambuí (Goiás-Brésil). *Anais Academia Brasileira Ciências*, *48*, 555–566.

de Morrison Valeriano, C. (2016). The southern Brasília belt. In M. Heilbron, U. G. Cordani, & F. F. Alkmim (Eds.), *São Francisco Craton, Eastern Brazil: Tectonic genealogy of a miniature continent* (pp. 189–203). Springer.

Derry, L. A. (2015). Causes and consequences of mid-Proterozoic anoxia. *Geophysical Research Letters*, *42*, 8538–8546. https://doi.org/10.1002/2015GL065333

Fairchild, T. R., Schopf, J. W., Shen-Miller, J., Guimarães, E. M., Edwards, M. D., Lagstein, A., Li, X., Pabst, M., & de Melo-Filho, L. S. (1996). Recent discoveries of Proterozoic microfossils in south-central Brazil. *Precambrian Research*, *80*, 125–152. https://doi.org/10.1016/S0301-9268(96)00009-5

Fakhraee, M., Hancisse, O., Canfield, D. E., Crowe, S. A., & Katsev, S. (2019). Proterozoic seawater sulfate scarcity and the evolution of ocean–atmosphere chemistry. *Nature Geoscience*, *12*, 375–380. https://doi.org/10.1038/s41561-019-0351-5

Fike, D. A., Bradley, A. S., & Rose, C. V. (2015). Rethinking the ancient sulfur cycle. *Annual Review of Earth and Planetary Sciences*, *43*, 593–622. https://doi.org/10.1146/annurev-earth-060313-054802

Freudenthal, T., Wagner, T., Wenzhoefer, F., Zabel, M., & Wefer, G. (2001). Early diagenesis of organic matter from sediments of the eastern subtropical Atlantic: Evidence from stable nitrogen and carbon isotopes. *Geochimica Et Cosmochimica Acta*, *65*, 1795–1808. https://doi.org/10.1016/S0016-7037(01)00554-3

Fuck, R. A., Marini, O. J., Dardenne, M. A., & de Figueiredo, A. N. (1988). Coberturas metassedimentares do Proterozoico Médio: os grupos Araí e Paranoá na região de Niquelândia-Colinas, Goiás. *Revista Brasileira De Geociências*, *18*, 54–62.

Fulton, J. M., Arthur, M. A., & Freeman, K. H. (2012). Black Sea nitrogen cycling and the preservation of phytoplankton $\delta^{15}N$ signals during the Holocene. *Global Biogeochemical Cycles*, *26*, GB2030.

Gault-Ringold, M., Adu, T., Stirling, C. H., Frew, R. D., & Hunter, K. A. (2012). Anomalous biogeochemical behavior of cadmium in subantarctic surface waters Mechanistic constraints from cadmium isotopes. *Earth and Planetary Science Letters*, *341*, 94–103. https://doi.org/10.1016/j.epsl.2012.06.005

George, E., Stirling, C. H., Gault-Ringold, M., Ellwood, M. J., & Middag, R. (2019). Marine biogeochemical cycling of cadmium and cadmium isotopes in the extreme nutrient-depleted subtropical gyre of the South West Pacific Ocean. *Earth and Planetary Science Letters*, *514*, 84–95. https://doi.org/10.1016/j.epsl.2019.02.031

Gilleaudeau, G. J., & Kah, L. C. (2015). Heterogeneous redox conditions and a shallow chemocline in the Mesoproterozoic ocean: Evidence from carbon–sulfur–iron relationships. *Precambrian Research*, *257*, 94–108. https://doi.org/10.1016/j.precamres.2014.11.030

Gilleaudeau, G. J., Sahoo, S. K., Ostrander, C. M., Owens, J. D., Poulton, S. W., Lyons, T. W., & Anbar, A. D. (2020). Molybdenum isotope and trace metal signals in an iron-rich Mesoproterozoic ocean: A snapshot from the Vindhyan Basin, India. *Precambrian Research*, *343*, 105718. https://doi.org/10.1016/j.precamres.2020.105718

Gomes, M. L., & Hurtgen, M. T. (2013). Sulfur isotope systematics of a euxinic, low-sulfate lake: Evaluating the importance of the reservoir effect in modern and ancient oceans. *Geology*, *41*, 663–666. https://doi.org/10.1130/G34187.1

Gomes, M. L., & Hurtgen, M. T. (2015). Sulfur isotope fractionation in modern euxinic systems: Implications for paleoenvironmental reconstructions of paired sulfate–sulfide isotope records. *Geochimica Et Cosmochimica Acta*, *157*, 39–55. https://doi.org/10.1016/j.gca.2015.02.031

Guinoiseau, D., Galer, S. J. G., & Abouchami, W. (2018). Effect of cadmium sulphide precipitation on the partitioning of Cd isotopes: Implications for the oceanic Cd cycle. *Earth and Planetary Science Letters*, *498*, 300–308. https://doi.org/10.1016/j.epsl.2018.06.039

Guinoiseau, D., Galer, S. J. G., Abouchami, W., Frank, M., Achterberg, E. P., & Haug, G. H. (2019). Importance of cadmium sulfides for biogeochemical cycling of Cd and its isotopes in Oxygen Deficient Zones – A case study of the Angola Basin. *Global Biogeochemical Cycles*, *33*(12), 1746–1763. https://doi.org/10.1029/2019gb006323

Gutzmer, J., & Beukes, N. J. (1998). Earliest laterites and possible evidence for terrestrial vegetation in the Early Proterozoic. *Geology*, *26*, 263–266.

Haendel, D., Muehle, K., Nitzsche, H.-M., Stiehl, G., & Wand, U. (1986). Isotopic variations of the fixed nitrogen in metamorphic rocks. *Geochimica Et Cosmochimica Acta*, *50*, 749–758. https://doi.org/10.1016/0016-7037(86)90351-0

Hao, J., Knoll, A. H., Huang, F., Hazen, R. M., & Daniel, I. (2020). Cycling phosphorus on the Archean Earth: Part I. Continental weathering and riverine transport of phosphorus. *Geochimica Et Cosmochimica Acta*, *273*, 70–84. https://doi.org/10.1016/j.gca.2020.01.027

Hao, J., Sverjensky, D. A., & Hazen, R. M. (2017). Mobility of nutrients and trace metals during weathering in the late Archean. *Earth and Planetary Science Letters*, *471*, 148–159. https://doi.org/10.1016/j.epsl.2017.05.003

Hardisty, D. S., Lu, Z., Bekker, A., Diamond, C. W., Gill, B. C., Jiang, G., Kah, L. C., Knoll, A. H., Loyd, S. J., Osburn, M. R., Planavsky, N. J., Wang, C., Zhou, X., & Lyons, T. W. (2017). Perspectives on Proterozoic surface ocean redox from iodine contents in ancient and recent carbonate. *Earth and Planetary Science Letters*, *463*, 159–170. https://doi.org/10.1016/j.epsl.2017.01.032

Hodgskiss, M. S., Sansjofre, P., Kunzmann, M., Sperling, E. A., Cole, D. B., Crockford, P. W., Gibson, T. M., & Halverson, G. P. (2020). A high-TOC shale in a low productivity world: The late Mesoproterozoic Arctic Bay Formation, Nunavut. *Earth and Planetary Science Letters*, *544*, 116384. https://doi.org/10.1016/j.epsl.2020.116384

Hohl, S. V., Galer, S. J. G., Gamper, A., & Becker, H. (2017). Cadmium isotope variations in Neoproterozoic carbonates - A tracer of biologic production? *Geochemical Perspectives Letters*, *3*, 32–44. https://doi.org/10.7185/geochemlet.1704

Hohl, S. V., Jiang, S.-Y., Viehmann, S., Wei, W., Liu, Q., Wei, H.-Z., & Galer, S. J. G. (2020). Trace metal and Cd isotope systematics of the basal datangpo formation, Yangtze Platform (South China) indicate restrained (Bio)Geochemical metal cycling in Cryogenian seawater. *Geosciences*, *10*, 27–36. https://doi.org/10.3390/geosciences10010036

Hohl, S. V., Jiang, S.-Y., Wei, H.-Z., Pi, D.-H., Liu, Q., Viehmann, S., & Galer, S. J. G. (2019). Cd isotopes trace periodic (bio)geochemical metal cycling at the verge of the Cambrian animal evolution. *Geochimica Et Cosmochimica Acta*, *263*, 195–214. https://doi.org/10.1016/j.gca.2019.07.036

Javaux, E. J., Knoll, A. H., & Walter, M. R. (2001). Morphological and ecological complexity in early eukaryotic ecosystems. *Nature*, *412*, 66–69. https://doi.org/10.1038/35083562

Kah, L. C., Lyons, T. W., & Frank, T. D. (2004). Low marine sulphate and protracted oxygenation of the Proterozoic biosphere. *Nature*, *431*, 834–838. https://doi.org/10.1038/nature02974

Kessler, A. J., Bristow, L. A., Cardenas, M. B., Glud, R. N., Thamdrup, B., & Cook, P. L. (2014). The isotope effect of denitrification in permeable sediments. *Geochimica Et Cosmochimica Acta*, *133*, 156–167. https://doi.org/10.1016/j.gca.2014.02.029

Kipp, M. A., & Stüeken, E. E. (2017). Biomass recycling and Earth's early phosphorus cycle. *Science Advances*, *3*, eaao4795. https://doi.org/10.1126/sciadv.aao4795

Kipp, M. A., Stüeken, E. E., Yun, M., Bekker, A., & Buick, R. (2018). Pervasive aerobic nitrogen cycling in the surface ocean across the Paleoproterozoic Era. *Earth and Planetary Science Letters*, *500*, 117–126. https://doi.org/10.1016/j.epsl.2018.08.007

Knoll, A. H., & Nowak, M. A. (2017). The timetable of evolution. *Science Advances*, *3*, e1603076. https://doi.org/10.1126/sciadv.1603076

Koehler, M. C., Stüeken, E. E., Kipp, M. A., Buick, R., & Knoll, A. H. (2017). Spatial and temporal trends in Precambrian nitrogen cycling: A Mesoproterozoic offshore nitrate minimum. *Geochimica Et Cosmochimica Acta*, *198*, 315–337. https://doi.org/10.1016/j.gca.2016.10.050

Kritee, K., Sigman, D. M., Granger, J., Ward, B. B., Jayakumar, A., & Deutsch, C. (2012). Reduced isotope fractionation by denitrification under conditions relevant to the ocean. *Geochimica Et Cosmochimica Acta*, *92*, 243–259. https://doi.org/10.1016/j.gca.2012.05.020

Lacan, F., Francois, R., Ji, Y., & Sherrell, R. M. (2006). Cadmium isotopic composition in the ocean. *Geochimica Et Cosmochimica Acta*, *70*, 5104–5118. https://doi.org/10.1016/j.gca.2006.07.036

Lam, P., & Kuypers, M. M. (2011). Microbial nitrogen cycling processes in oxygen minimum zones. *Annual Rreview of Marine Science*, *3*, 317–345. https://doi.org/10.1146/annurev-marine-120709-142814

Lehman, M. R., Bernasconi, S. M., Barbieri, A., & McKenzie, J. A. (2002). Preservation of organic matter and alteration of its carbon and nitrogen isotope composition during simulated and in situ early

sedimentary diagenesis. *Geochimica Et Cosmochimica Acta*, *66*, 3573–3584. https://doi.org/10.1016/S0016-7037(02)00968-7

Leventhal, J. S. (1983). An interpretation of carbon and sulfur relationships in Black Sea sediments as indicators of environments of deposition. *Geochimica Et Cosmochimica Acta*, *47*, 133–137. https://doi.org/10.1016/0016-7037(83)90097-2

Luo, G., Ono, S., Huang, J., Algeo, T. J., Li, C., Zhou, L., Robinson, A., Lyons, T. W., & Xie, S. (2014). Decline in oceanic sulfate levels during the early Mesoproterozoic. *Precambrian Research*, *258*, 36–47. https://doi.org/10.1016/j.precamres.2014.12.014

Lyons, T. W., Reinhard, C. T., & Planavsky, N. J. (2014). The rise of oxygen in Earth's early ocean and atmosphere. *Nature*, *506*, 307–315. https://doi.org/10.1038/nature13068

Matteini, M., Dantas, E. L., Pimentel, M. M., de Alvarenga, C. J. S., & Dardenne, M. A. (2012). U-Pb and Hf isotope study on detrital zircons from the Paranoá Group, Brasília Belt Brazil: Constraints on depositional age at Mesoproterozoic-Neoproterozoic transition and tectono-magmatic events in the São Francisco craton. *Precambrian Research*, *206*, 168–181. https://doi.org/10.1016/j.precamres.2012.03.007

Moebius, J. (2013). Isotope fractionation during nitrogen remineralization (ammonification): implications for nitrogen isotope biogeochemistry. *Geochimica Et Cosmochimica Acta*, *105*, 422–432. https://doi.org/10.1016/j.gca.2012.11.048

Pang, K., Tang, Q., Wu, C., Li, G., Chen, L., Wan, B., Yuan, X., Bodnar, R. J., & Xiao, S. (2020). Raman spectroscopy and structural heterogeneity of carbonaceous material in Proterozoic organic-walled microfossils in the North China Craton. *Precambrian Research*, *346*, 105818. https://doi.org/10.1016/j.precamres.2020.105818

Peters, S. E., & Husson, J. M. (2017). Sediment cycling on continental and oceanic crust. *Geology*, *45*, 323–326. https://doi.org/10.1130/G38861.1

Pimentel, M. M., Fuck, R. A., & Botelho, N. F. (1999). Granites and the geodynamic history of the Neoproterozoic Brasılia belt, central Brazil: A review. *Lithos*, *46*, 463–483.

Pimentel, M. M., Rodrigues, J. B., DellaGiustina, M. E. S., Junges, S., Matteini, M., & Armstrong, R. (2011). The tectonic evolution of the Neoproterozoic Brasília Belt, central Brazil, based on SHRIMP and LA-ICPMS U-Pb sedimentary provenance data: a review. *Journal of South American Earth Sciences*, *31*, 345–357. https://doi.org/10.1016/j.jsames.2011.02.011

Planavsky, N. J., Bekker, A., Rouxel, O. J., Kamber, B., Hofmann, A., Knudsen, A., & Lyons, T. W. (2010). Rare Earth Element and yttrium compositions of Archean and Paleoproterozoic Fe formations revisited: New perspectives on the significance and mechanisms of deposition. *Geochimica Et Cosmochimica Acta*, *74*, 6387–6405. https://doi.org/10.1016/j.gca.2010.07.021

Planavsky, N. J., McGoldrick, P., Scott, C. T., Li, C., Reinhard, C. T., Kelly, A. E., Chu, X., Bekker, A., Love, G. D., & Lyons, T. W. (2011). Widespread iron-rich conditions in the mid-Proterozoic ocean. *Nature*, *477*, 448–451. https://doi.org/10.1038/nature10327

Poulton, S. W., Fralick, P. W., & Canfield, D. E. (2010). Spatial variability in oceanic redox structure 1.8 billion years ago. *Nature Geoscience*, *3*, 486–490.

Reinhard, C. T., Planavsky, N. J., Gill, B. C., Ozaki, K., Robbins, L. J., Lyons, T. W., Fischer, W. W., Wang, C., Cole, D. B., & Konhauser, K. O. (2017). Evolution of the global phosphorus cycle. *Nature*, *541*, 386–389. https://doi.org/10.1038/nature20772

Reinhard, C. T., Planavsky, N., Olson, S. L., Lyons, T. W., & Erwin, D. H. (2016). Earth's oxygen cycle and the evolution of animal life. *Proceedings of the National Academy of Sciences of the United States of America*, *113*(32), 8933–8938. https://doi.org/10.1073/pnas.1521544113

Reinhard, C. T., Planavsky, N. J., Robbins, L. J., Partin, C. A., Gill, B. C., Lalonde, S. V., Bekker, A., Konhauser, K. O., & Lyons, T. W. (2013). Proterozoic ocean redox and biogeochemical stasis. *Proceedings of the National Academy of Sciences of the United States of America*, *110*, 5357–5362. https://doi.org/10.1073/pnas.1208622110

Ripperger, S., Rehkämper, M., Porcelli, D., & Halliday, A. N. (2007). Cadmium isotope fractionation in seawater — A signature of biological activity. *Earth and Planetary Science Letters*, *261*, 670–684. https://doi.org/10.1016/j.epsl.2007.07.034

Robinson, R. S., Kienast, M., Albuquerque, A. L., Altabet, M., Contreras, S., De Pol, H. R., Dubois, N., Francois, R., Galbraith, E., Shu, T.-C., Ivanochko, T., Jaccard, S., Kao, S.-J., Kiefer, T., Kienast, S., Lehmann, M., Martinez, P., McCarthy, M., Moebius, J., … Yang, J.-Y. (2012). A review of nitrogen isotopic alteration in marine sediments. *Paleoceanography*, *27*, PA4203. https://doi.org/10.1029/2012PA002321

Rooze, J., & Meile, C. (2016). The effect of redox conditions and bioirrigation on nitrogen isotope fractionation in marine sediments. *Geochimica Et Cosmochimica Acta*, *184*, 227–239. https://doi.org/10.1016/j.gca.2016.04.040

Sánchez-Baracaldo, P., Raven, J. A., Pisani, D., & Knoll, A. H. (2017). Early photosynthetic eukaryotes inhabited low-salinity habitats. *Proceedings of the National Academy of Sciences of the United States of America*, *114*(37), E7737–E7745. https://doi.org/10.1073/pnas.1620089114

Sayle, K. L., Brodie, C. R., Cook, G. T., & Hamilton, W. D. (2019). Sequential measurement of δ15N, δ13C and δ34S values in archaeological bone collagen at the Scottish Universities Environmental Research Centre (SUERC): a new analytical frontier. *Rapid Communications in Mass Spectrometry*, *33*, 1258–1266.

Schidlowski, M. (2001). Carbon isotopes as biogeochemical recorders of life over 3.8 Ga of Earth history: Evolution of a concept. *Precambrian Research*, *106*, 117–134. https://doi.org/10.1016/S0301-9268(00)00128-5

Schmitt, A.-D., Galer, S. J. G., & Abouchami, W. (2009). Mass-dependent cadmium isotopic variations in nature with emphasis on the marine environment. *Earth and Planetary Science Letters*, *277*, 262–272. https://doi.org/10.1016/j.epsl.2008.10.025

Shen, Y., Canfield, D. E., & Knoll, A. H. (2002). Middle Proterozoic ocean chemistry: Evidence from the McArthur Basin, Northern Australia. *American Journal of Science*, *302*, 81–109. https://doi.org/10.2475/ajs.302.2.81

Shen, Y., Knoll, A. H., & Walter, M. R. (2003). Evidence for low sulphate and anoxia in a mid-Proterozoic marine basin. *Nature*, *423*, 632–635. https://doi.org/10.1038/nature01651

Sieber, M., Conway, T. M., de Souza, G. F., Obata, H., Takano, S., Sohrin, Y., & Vance, D. (2019). Physical and biogeochemical controls on the distribution of dissolved cadmium and its isotopes in the Southwest Pacific Ocean. *Chemical Geology*, *511*, 494–509. https://doi.org/10.1016/j.chemgeo.2018.07.021

Sim, M. S., Bosak, T., & Ono, S. (2011). Large sulfur isotope fractionation does not require disproportionation. *Science*, *333*, 74–77. https://doi.org/10.1126/science.1205103

Sindol, G. P., Babechuk, M. G., Petrus, J. A., & Kamber, B. S. (2020). New insights into Paleoproterozoic surficial conditions revealed by 1.85 Ga corestone-rich saprolith. *Chemical Geology*, *545*, 119621.

Strother, P. K., Battison, L., Brasier, M. D., & Wellman, C. H. (2011). Earth's earliest non-marine eukaryotes. *Nature*, *473*, 505–509. https://doi.org/10.1038/nature09943

Stüeken, E. E. (2013). A test of the nitrogen-limitation hypothesis for retarded eukaryote radiation: nitrogen isotopes across a Mesoproterozoic basinal profile. *Geochimica Et Cosmochimica Acta*, *120*, 121–139. https://doi.org/10.1016/j.gca.2013.06.002

Stüeken, E. E., de Castro, M., Krotz, L., Brodie, C., Iammarino, M., & Giazzi, G. (2020). Optimized switch-over between CHNS abundance and CNS isotope ratio analyses by elemental analyzer-isotope ratio mass spectrometry: Application to six geological reference materials. *Rapid Communications in Mass Spectrometry*, *34*(18), e8821. https://doi.org/10.1002/rcm.8821

Stüeken, E. E., Kipp, M. A., Koehler, M. C., & Buick, R. (2016). The evolution of Earth's biogeochemical nitrogen cycle. *Earth Science Reviews*, *160*, 220–239. https://doi.org/10.1016/j.earscirev.2016.07.007

Tepe, N., & Bau, M. (2016). Behavior of rare earth elements and yttrium during simulation of arctic estuarine mixing between glacial-fed riverwaters and seawater and the impact of inorganic (nano-)particles. *Chemical Geology*, *438*, 134–145. https://doi.org/10.1016/j.chemgeo.2016.06.001

Tesdal, J. E., Galbraith, E. D., & Kienast, M. (2013). Nitrogen isotopes in bulk marine sediment: Linking seafloor observations with subseafloor records. *Biogeosciences*, *10*, 101–118. https://doi.org/10.5194/bg-10-101-2013

Thomazo, C., Couradeau, E., & Garcia-Pichel, F. (2018). Possible nitrogen fertilization of the early Earth Ocean by microbial continental ecosystems. *Nature Communications*, *9*, 1–8. https://doi.org/10.1038/s41467-018-04995-y

Thomazo, C., & Papineau, D. (2013). Biogeochemical cycling of nitrogen on the early Earth. *Elements*, *9*, 345–351. https://doi.org/10.2113/gselements.9.5.345

Thomazo, C., Pinti, D. L., Busigny, V., Ader, M., Hashizume, K., & Phillippot, P. (2009). Biological activity and the Earth's surface evolution: Insights from carbon, sulfur, nitrogen and iron stable isotopes in the rock record. *Comptes Rendus Palevol*, *8*, 665–678. https://doi.org/10.1016/j.crpv.2009.02.003

Thunell, R. C., Sigman, D. M., Muller-Karger, F., Astor, Y., & Varela, R. (2004). Nitrogen isotope dynamics of the Cariaco Basin, Venezuela. *Global Biogeochemical Cycles*, *18*, GB3001. https://doi.org/10.1029/2003GB002185

Viehmann, S., Hohl, S. V., Kraemer, D., Bau, M., Walde, D. H., Galer, S. J., Jiang, S. Y., & Meister, P. (2019). Metal cycling in Mesoproterozoic microbial habitats: Insights from trace elements and stable Cd isotopes in stromatolites. *Gondwana Research*, *67*, 101–114. https://doi.org/10.1016/j.gr.2018.10.014

Wang, Z., Wang, X., Shi, X., Tang, D., Stüeken, E. E., & Song, H. (2020). Coupled Nitrate and Phosphate Availability Facilitated the Expansion of Eukaryotic Life at Circa 1.56 Ga. *Journal of Geophysical Research Biogeosciences*, *125*, e2019JG005487. https://doi.org/10.1029/2019JG005487

Wei, W., & Algeo, T. J. (2019). Elemental proxies for paleosalinity analysis of ancient shales and mudrocks. *Geochimica Et Cosmochimica Acta*, *287*, 341–366.

Wotte, T., Shields-Zhou, G. A., & Strauss, H. (2012). Carbonate-associated sulfate: Experimental comparisons of common extraction methods and recommendations toward a standard analytical protocol. *Chemical Geology*, *326*, 132–144. https://doi.org/10.1016/j.chemgeo.2012.07.020

Xie, R. C., Rehkämper, M., Grasse, P., van de Flierdt, T., Frank, M., & Xue, Z. (2019). Isotopic evidence for complex biogeochemical cycling of Cd in the eastern tropical South Pacific. *Earth and Planetary Science Letters*, *512*, 134–146. https://doi.org/10.1016/j.epsl.2019.02.001

Zhang, X., Sigman, D. M., Morel, F. M., & Kraepiel, A. M. (2014). Nitrogen isotope fractionation by alternative nitrogenases and past ocean anoxia. *Proceedings of the National Academy of Sciences of the United States of America*, *111*, 4782–4787. https://doi.org/10.1073/pnas.1402976111

Zhang, X., Ward, B. B., & Sigman, D. M. (2020). Global nitrogen cycle: Critical enzymes, organisms, and processes for nitrogen budgets and dynamics. *Chemical Reviews*, *120*, 5308–5351. https://doi.org/10.1021/acs.chemrev.9b00613

How to cite this article: Stüeken, E. E., Viehmann, S., & Hohl, S. V. (2021). Contrasting nutrient availability between marine and brackish waters in the late Mesoproterozoic: Evidence from the Paranoá Group, Brazil. *Geobiology*, 00, 1–16. https://doi.org/10.1111/gbi.12478